RSC Advances

PAPER

View Article Online
View Journal | View Issue

Cite this: *RSC Adv.*, 2017, **7**, 34118

Amphiphilic silane modified multifunctional nanoparticles for ratiometric oxygen sensing†

Yanxia Lin,‡ Hongwei Xu,‡ Biao Dong,* Xueke Sun, Chunhe Li, Jianing Li, Lin Xu, Xue Bai and Hongwei Song

Received 10th May 2017
Accepted 27th June 2017

DOI: 10.1039/c7ra05282k

rsc.li/rsc-advances

Precise detection of dissolved oxygen (DO) at the cellular level plays a pivotal role in the diagnosis of many diseases and intraoperative observation. In this work, we designed a ratiometric fluorescence DO sensing probe based on efficient energy transfer at long wavelength excitation. The oxygen probe Pt(II)-*meso*-tetra(pentafluorophenyl)porphine (PtTFPP), the reference dye Coumarin 6 (C6) and Fe_3O_4 NPs were encapsulated by amphiphilic silane at room temperature. The results indicate the important role of C6 molecules in the composite, serving as not only the ratiometric reference probe, but also the sensitizer of efficient energy transfer. The emission from PtTFPP can be greatly enhanced by 20 times based on the energy transfer pathway from C6 relative to that with the intrinsic excitation wavelength. DO sensing was successfully carried out based on ratiometric fluorescence in the imitation environment and at the cellular level under a confocal microscope. In addition, the cell magnetic separation function makes the composite possess great potential in DO sensing related medical applications.

Introduction

Oxygen is an essential component for many physiological and pathological processes in living cells.[1,2] It has been reported that tissue hypoxia is closely related to the clinical course of a variety of diseases,[3–8] such as tumor growth,[9,10] diabetic retinopathy[11] and rheumatoid arthritis.[12] A lot of efforts have been made in the development of oxygen sensors,[13–16] while the measurement and monitoring of oxygen levels in living cells and tissue are still a challenge when facing modern biology, physiology and medicine. In recent years, optical oxygen sensors based on luminescence quenching[17,18] have shown significant advantages of high sensitivity, low detection limit and noninvasive character relative to other methods, such as the classical Winkler titration, electroanalytical, pressure-based and lifetime detection.[19] Besides, it can be implemented for real-time measurements as well as higher solution oxygen mapping in tissues.[20–23]

Organometallic complexes and metalloporphyrins[24,25] are the most famous optical sensing probes for oxygen due to the quenching effect. Single-intensity-based oxygen sensing is the conventional way, which, however, is hard to give quantitative information since it is necessary but difficult to confirm both the precise concentration of probe and analyte at the same time.[26] Therefore, the ratiometric oxygen sensors are designed by incorporating reference-probe dual-dye systems into an inert matrix in the form of sensor strips,[27] films,[28] microparticles[29] and nanoparticles (NPs),[21,29–31] where the oxygen sensing can be obtained by ratiometric approaches, *i.e.* simultaneously detecting two signals by a single excitation wavelength.[26] K. A. Van Houten *et al.*[32] first developed an oxygen-sensitive dyes, possessing two distinct emission peaks with differing sensitivity to oxygen quenching, platinum 1,2-enedithiolates and further applied it in the DO sensing by a ratiometric method. After that, the ratiometric detection makes a rapid progress. Jason McNeill and Wu *et al.*[33] designed a novel nanoparticle architecture for ratiometric fluorescence oxygen sensing that consisted of p-conjugated polymer molecules doped with an oxygen-sensitive dye. Besides, they observed the efficient energy transfer from the polymer to phosphorescent dye upon light excitation, resulting in bright phosphorescence. Peng and Wolfbeis *et al.*[34] further developed a method to assess tumor mitochondrial dysfunction with three phosphorescent nanosensors, which responded to the oxygen among the subcellular organelles.

As the in-depth study, to meet the requirements of the clinic applications, the DO sensing probe should have some features on consideration of low toxicity, high efficiency and sensitivity in the live cell or tissue environments, such as long wavelength excitation, well designed combination of oxygen probe and reference-probe. In addition, the multifunction design of the probe also becomes an important issue for the theranostic applications.

In this work, we designed a multifunctional oxygen probes based on amphiphilic silane modification method we recently

State Key Laboratory on Integrated Optoelectronics, College of Electronic Science and Engineering, Jilin University, 2699 Qianjin Street, Changchun, 130012, P. R. China. E-mail: dongb@jlu.edu.cn

† Electronic supplementary information (ESI) available. See DOI: 10.1039/c7ra05282k

‡ These authors contributed equally to this work and should be considered co-first authors.

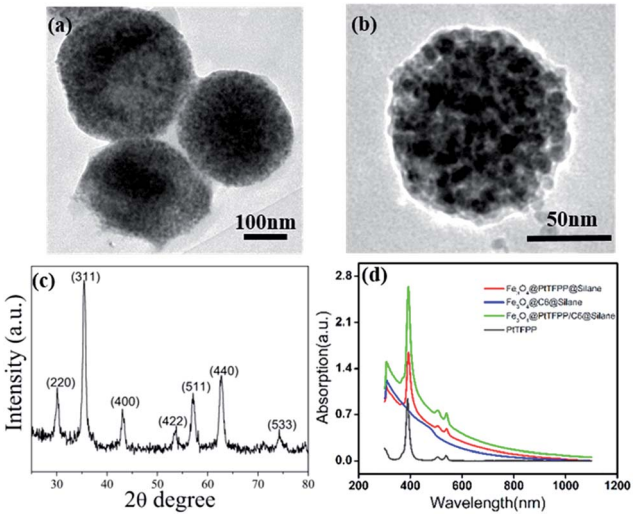

Fig. 1 (a) TEM images of (a) Fe_3O_4@PtTFPP/C6@silane NPs and (b) one single Fe_3O_4@PtTFPP/C6@silane NP. (c) The XRD pattern of Fe_3O_4 NPs accorded with JCPDS 6563107. (d) UV-Vis absorption spectra of Fe_3O_4@PtTFPP@silane, Fe_3O_4@C6@silane, Fe_3O_4@PtTFPP/C6@silane and pure PtTFPP.

developed for multifunctional platform, which can encapsulate the hydrophobic functional molecules by hydrophobic interaction, while the outside hydrophilic hydroxy can facilitate the bioapplications. The oxygen probe Pt(II)-*meso*-tetra(pentafluorophenyl)porphine (PtTFPP) and the reference dye of Coumarin 6 (C6) were encapsulated inside the hydrophobic environment of silane *via* the hydrolysis reaction, as the ratiometric sensing system, both of which can share the same excitation wavelength. In addition, the iron oxide nanoparticles (IONPs) with ultrasmall size were also employed as core together with PtTFPP and C6 molecules, and the composite was called as Fe_3O_4@PtTFPP/C6@silane. The whole preparation process is described in Fig. 1. The multifunction design holds the advantages of magnetic separation of cells and cellar ratiometric oxygen sensing. What's more, we first found the efficient energy transfer from C6 to PtTFPP with the excitation at 458 nm, which shows higher luminescent intensity and much more harmless to the cells relative to that intrinsic excitation at UV area.

Materials and methods

Materials

The oxygen probe Pt(II)-*meso*-tetra(pentafluorophenyl)porphine (PtTFPP), the reference dye Coumarin 6 (C6), trimethoxy(octadecyl)silane, $FeCl_3 \cdot 6H_2O$, $FeCl_2 \cdot 4H_2O$, glucose, glucose oxidase and tetrahydrofuran (THF) 3-(4,5-dimethylthiazol-2-yl)-2,15-diphenyltetrazolium bromide (MTT) assay were purchased from Sigma-Aldrich (http://www.sigmaaldrich.com). All chemicals were used without further purification. Doubly distilled water was used in all experiments.

Synthesis of magnetic OA–Fe_3O_4 NPs

Magnetic OA–Fe_3O_4 NPs were synthesized following a recipe as below. Firstly, $FeCl_3 \cdot 6H_2O$ (5.38 g) was resolved in deionized water (200 mL) in three-necked flask for 10 min nitrogen gas protection. Then $FeCl_2 \cdot 4H_2O$ (1.98 g) was added into the former solution with the color changing to orange immediately. After 10 min, ammonium hydroxide solution (25%, 7 mL) was injected into the three-necked flask with vigorous stirring, and the color of the mixture changed to black instantly. The solution was stirred for an additional 3 hours at room temperature and then washed with deionized water for three times. The black product was dissolved in 200 mL of deionized water with oleic acid (OA, 1.22 g) dropwise added. The mixture was heated to 80 °C for 30 min with stirring under a flow of nitrogen. The OA–Fe_3O_4 NPs were dissolved in hexane for further experiments.

Synthesis of silane-modified OA–Fe_3O_4 NPs loading with C6 and PtTFPP

The OA–Fe_3O_4 NPs (5 mg mL^{-1}, 40 μL), trimethoxy(octadecyl) silane (7.5 mg mL^{-1}, 100 μL), the reference dye Coumarin 6 (C6, 1 mg mL^{-1}, 50 μL) and PtTFPP (1 mg mL^{-1}, 60 μL) were mixed in tetrahydrofuran (THF) under sonication. After 10 minutes, mixing solution was rapidly injected to 5 mL water (pH ≈ 9, adjusted by addition of ammonium hydroxide) in a conical flask for the hydrolyse process. Then the conical flask was put in a water bath at 30 °C for 4 h, and the resolution was dialyzed for 24 h at room temperature. In the end, Fe_3O_4@PtTFPP/C6@silane NPs were finished.

Cell culture

The MCF-7 cells were purchased from Shanghai Institute for Biological Sciences Chinese Academy of Science, and were cultured in culture medium RPMI 1640 (Hyclone) supplemented with 10% fetal bovine serum (FBS, Clark) and 1% penicillin–streptomycin (100 U mL^{-1} penicillin and 100 g mL^{-1} streptomycin), in an incubator with 5% CO_2 and 100% humidity at 37 °C. Cells in the exponential phase of growth were used in all the experiments.

Cytotoxicity assay

For the *in vitro* cytotoxicity test, MCF-7 cells were cultured in RPMI-1640 medium containing 10% fetal bovine serum (FBS) and 1% penicillin/streptomycin under 37 °C within 5% CO_2 atmosphere. 3-(4,5-Dimethylthiazol-2-yl)-2,15-diphenyltetrazolium bromide (MTT) assay was used to determine the cytotoxicity at various mass concentrations of samples. MCF-7 cells were seeded in 96-well plates at 1 × 104 per well and cultured for 24 h. Then Fe_3O_4@PtTFPP/C6@silane were added to cells for another 24 h. After adding 10 μL of 5 mg mL^{-1} MTT solution for a further 4 h incubation (37 °C), the medium was carefully removed, and 150 μL of dimethyl sulfoxide was added. After 10–20 min dissolution, the absorbance at 490 nm was recorded using a microplate reader (Bio-Tek ELX800, USA).

Femtosecond transient absorption setup

The TA setup consisted of 400 nm pump pulses doubled from 800 nm laser pulses (~100 fs duration, 250 Hz repetition rate)

generated from a mode-locked Ti: sapphire laser/amplifier system (Solstice, Spectra-Physics) and broadband white-light probe pulses generated from 2 mm-thick deuterated water. The relative polarization of the pump and the probe beams were set to the magic angle. The TA data were collected by a fiber-coupled spectra-meter connected to a computer. The group velocity dispersion of the transient spectra was compensated for using a chirp program. All the measurements were performed at room temperature. Pump-power dependent measurements were carried out. In the acceptable range, pump intensity independent dynamics were observed.[35]

Results and discussion

Synthesis and characterization of Fe_3O_4@PtTFPP/C6@silane NPs

The Scheme 1 shows the preparation process and cellar oxygen sensing application of composite Fe_3O_4@PtTFPP/C6@silane NPs. PtTFPP is a famous oxygen probe, which is greatly sensitive to the concentration of oxygen. Upon 405 nm excitation, PtTFPP yields highly oxygen-sensitive red phosphorescence with a good quenching response. Thus, by detecting the intensity of the 652 nm wavelength, can be detected by spectrometer and visualized from CLSM. C6 serves as a reference probe since it can be co-excited under 405 nm wavelength while is not sensitive to O_2. Amazingly, the co-loading of C6 can remarkably improve the luminescent intensity of PtTFPP at the wavelength of 652 nm under the highest excitation wavelength of 458 nm for C6, which is harmless for biological samples and efficient in the detection of oxygen. The inner magnetic Fe_3O_4 NPs offer the cell separation function, which is favorable for some certain cellular oxygen detention *via* magnetic navigation targeting to the tumor site or separation of circulating tumor cells in blood.

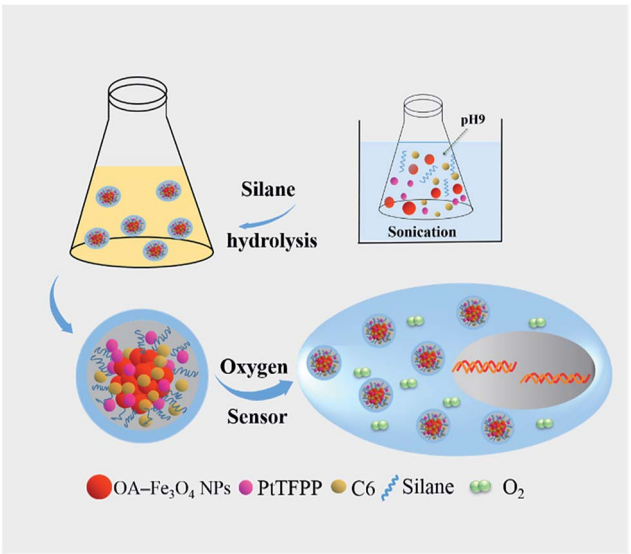

Scheme 1 Schematic representation of the synthesis of the Fe_3O_4@PtTFPP/C6@silane.

The TEM image of Fe_3O_4@PtTFPP/C6@silane in Fig. 1a shows basically spherical morphology after silane encapsulation with size of 120–150 nm. From the image of a single Fe_3O_4@PtTFPP/C6@silane particle in Fig. 1b, an aggregation of Fe_3O_4 NPs can be seen which happened in the hydrolysis process. The amphiphilic silane serves as coating layer and acts as the role of carrier, greatly improving the biocompatibility. Compared to other surface modification methods, this method is more simple and versatile without high temperature reaction.

The XRD pattern in Fig. 1c suggests the cubic crystalline structure of Fe_3O_4. From the UV-Vis absorption in Fig. 1d, the PtTFPP shows three bands at 400, 504 and 550 nm, respectively. After being encapsulated inside the composites, the bands of PtTFPP also appear in the absorption spectra of Fe_3O_4@PtTFPP@silane and Fe_3O_4@PtTFPP/C6@silane NPs, confirming the successful preparation of the composites. The zeta potential of the resulting NPs are −34.6 (Fig. S1†), showing highly solubility and stability.

Energy transfer in the Fe_3O_4@PtTFPP/C6@silane NPs

The excitation and emission spectra of pure PtTFPP, Fe_3O_4@PtTFPP@silane, Fe_3O_4@C6@silane and Fe_3O_4@PtTFPP/C6@silane are shown in Fig. 2a and b. Blue emission band centered at 510 nm belongs to C6 molecules, which can be excited by a wide band from 370 to 480 with the optimum wavelength of 458 nm. Fe_3O_4@PtTFPP@silane NPs show the red emission at 652 nm with three excitation bands centered at 390, 504 and 540 nm, respectively. The two molecules can be co-excited by the wavelength from 400 to 410 nm, since the C6 molecules play the role of reference probe. In this system, it is interesting that the excitation bands from 500 nm to 550 nm of PtTFPP molecules overlap with the emission band of C6 molecules, therefore, in Fe_3O_4@PtTFPP/C6@silane NPs, remarkable decrease of emission from C6 can be seen along with the obvious increase emission intensity of PtTFPP relative to the NPs with single molecule doping, which may be attributed to the energy transfer from C6 to PtTFPP molecules. Accordingly, in the excitation spectra of the Fe_3O_4@PtTFPP/C6@silane NPs, the excitation peak of C6 also appears while monitoring the emission of PtTFPP at 652 nm.

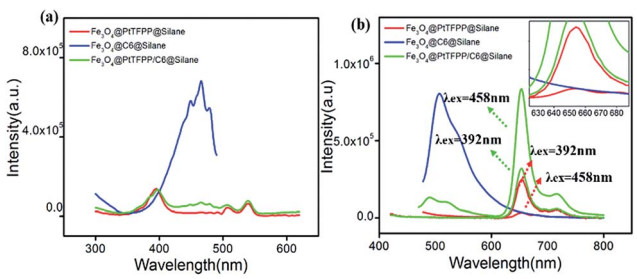

Fig. 2 (a) Excitation spectra of Fe_3O_4@PtTFPP@silane, Fe_3O_4@C6@silane and Fe_3O_4@PtTFPP/C6@silane NPs. (b) Emission spectra of 3 kinds of NPs (Fe_3O_4@PtTFPP@silane, Fe_3O_4@C6@silane, Fe_3O_4@PtTFPP/C6@silane) under 392 and 458 nm excitation. The inset shows the detail of the bottom area from 615 nm to 700 nm.

It is well known that long wavelength is more harmless to biological tissues than ultraviolet light. Therefore, Fe_3O_4@PtTFPP/C6@silane NPs with excitation wavelength at 458 nm can afford better DO sensing application in cellar level rather than 392 nm. Furthermore, based on the energy transfer from C6 to PtTFPP in Fe_3O_4@PtTFPP/C6@silane NPs, the red emission can be greatly enhanced. As shown in Fig. 2b, relative to the emission with the excitation of 392 nm, the red emission intensity experience a 3.6-fold increase by exciting C6 molecules at 458 nm based on energy transfer process. However, Fe_3O_4@PtTFPP@silane NPs without C6 (red lines in Fig. 2b) show very low emission with the excitation of 458 nm relative to that of 392 nm. Besides, compared with the emission of Fe_3O_4@PtTFPP@silane NPs with the excitation of 458 nm, the red emission intensity of Fe_3O_4@PtTFPP/C6@silane NPs shows a 20-fold increase by exciting C6 molecules based on energy transfer process. The results indicate the great contribution of C6 molecules in the luminescent property of the composite NPs.

Furthermore, we explored the ultrafast dynamics properties of the excited states using femtosecond broadband transient absorption (TA) spectroscopy. Fe_3O_4@C6@silane and Fe_3O_4@PtTFPP/C6@silane NPs with same amount of C6 (1 mg mL^{-1}, 50 μL) but different amount of PtTFPP (1 mg mL^{-1}, 60, 80, 100 μL) were excited at 458 nm, as shown in Fig. 3. The kinetics process of C6 at 500 nm was monitored. The lifetime value of Fe_3O_4@C6@silane NPs is 1.9 ns, while, with the increase amount of PtTFPP, the lifetime of C6 decreases accordingly. The corresponding lifetime of C6 are 1.51, 1.48, 1.10 ns by adding 60, 80, 100 μL PtTFPP, respectively. This phenomenon proves the energy transfer from C6 to PtTFPP.

The small organic molecules exhibited the concentration dependent luminescent properties in the composites. The emission spectra of Fe_3O_4@PtTFPP@silane NPs with different concentration of PtTFPP (1 mg mL^{-1}, 20, 40, 60, 80 μL) under excitation of 458 nm are displayed in Fig. 4a. Among the four samples Fe_3O_4@PtTFPP@silane NPs with 60 μL (1 mg mL^{-1}) PtTFPP show the highest emission intensity at 652 nm. Based on the optimum concentration of PtTFPP, the concentration of C6 was further investigated by tuning the amount of C6 (1 mg

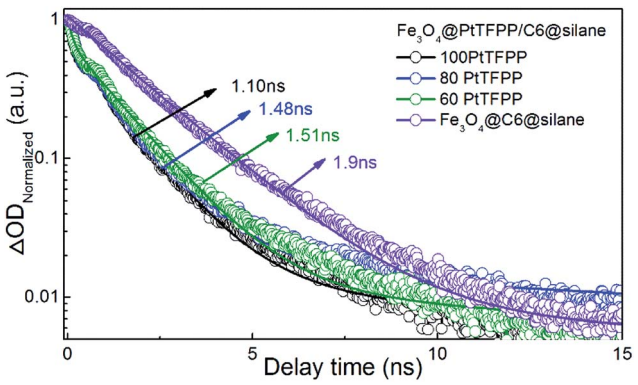

Fig. 3 Lifetime of C6 of 4 kinds of NPs (Fe_3O_4@C6@silane, Fe_3O_4@PtTFPP/C6@silane (PtTFPP, 1 mg mL^{-1}, 60 μL), Fe_3O_4@PtTFPP/C6@silane (PtTFPP, 1 mg mL^{-1}, 80 μL), Fe_3O_4@PtTFPP/C6@silane (PtTFPP, 1 mg mL^{-1}, 100 μL)).

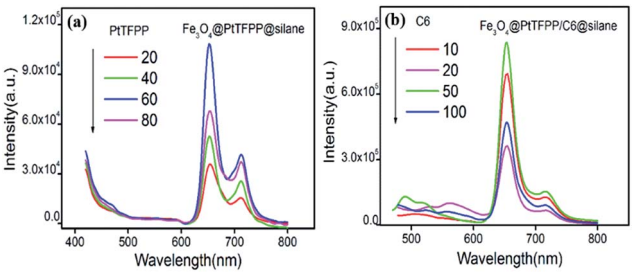

Fig. 4 (a) Emission spectra of Fe_3O_4@PtTFPP@silane NPs with different concentration of PtTFPP (1 mg mL^{-1}, 20, 40, 60, 80 μL) under 458 nm excitation. (b) Emission spectra of Fe_3O_4@PtTFPP/C6@silane NPs with different concentration of C6 (1 mg mL^{-1}, 10, 20, 50, 100 μL) under 458 nm excitation.

mL^{-1}, 10, 20, 50, 100 μL). As displayed in the Fig. 4b, Fe_3O_4@PtTFPP/C6@silane NPs with 50 μL (1 mg mL^{-1}) C6 have the highest intensity at 652 nm. Therefore, 50 μL (1 mg mL^{-1}) C6 was the proper concentration. In conclusion, Fe_3O_4@PtTFPP/C6@silane NPs with C6 and PtTFPP concentration of 60 μL (1 mg mL^{-1}) and 50 μL (1 mg mL^{-1}), respectively, were further used in the DO sensing.

Extracellular oxygen sensitivity of the Fe_3O_4@PtTFPP/C6@silane NPs

Oxygen sensitivity of the Fe_3O_4@PtTFPP/C6@silane NPs is studied by flowing a gas mixture with various N_2/O_2 ratios. As is displayed in Fig. 5a, emission of C6 at 500 and the PtTFPP at 652 nm can be seen. After introducing different amount of dissolved oxygen (DO), emission of PtTFPP is quenched, whereas the emission of C6 keeps stable. By defining R as the ratio of the emission intensity of PtTFPP (at 652 nm) to that of

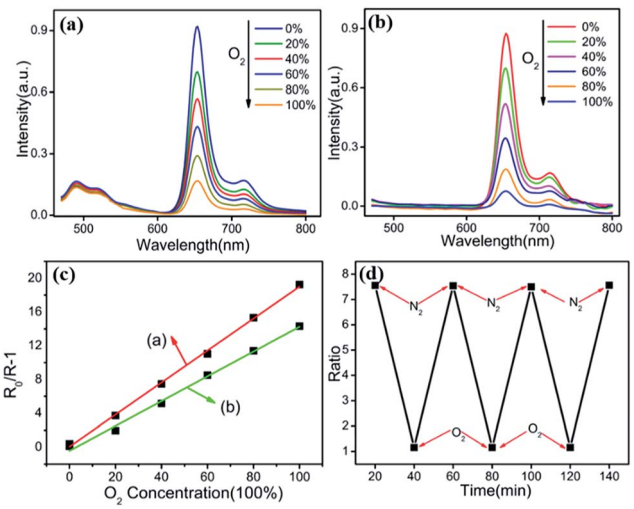

Fig. 5 (a and b) Ratiometric sensing with Fe_3O_4@PtTFPP/C6@silane and Fe_3O_4@PtTFPP@silane colloids, respectively. (c) Stern–Volmer plot of fluorescence intensity from (a and b). (d) Reversibility of Fe_3O_4@PtTFPP/C6@silane NPs responding to dissolved oxygen. The fluorescence ratios are plotted *versus* the experimental time.

C6 (at 500 nm), the sensitivity of the nanosensors can be expressed by the overall quenching response to DO,

$$Q = (R_{N_2} - R_{O_2})/R_{N_2}$$

where R_{N_2} and R_{O_2} respectively represent the emission intensity ratios of the sensor in fully deoxygenated and fully oxygenated solutions. The as-obtained value of Q for the hybrid sensing NPs is above 94%.

In bulky solid state systems, the oxygen-quenching process usually is described by the nonlinear Stern–Volmer equation due to matrix heterogeneity effects. In a nanoscale system, however, the large surface/volume ratio as well as the shortened penetration depth of oxygen virtually disregards the micro-heterogeneity of the local environment, and oxygen quenching can be expressed, as in a homogeneous system, by the linear Stern–Volmer equation,

$$R_0/R - 1 = K_{SV}[O_2]$$

where R_0 is the emission intensity ratio in the absence of oxygen, R as the ratio of a given oxygen concentration, K_{SV} as the Stern–Volmer quenching constant and $[O_2]$ as the DO concentration. Fig. 4c depicts the Stern–Volmer plot of the emission intensity ratios of NPs *versus* DO. In the whole range of oxygen concentration, the results fit very well with a correlation coefficient of >0.999, showing important potential of practical oxygen sensing.

The oxygen sensitivity of the Fe_3O_4@PtTFPP@silane NPs is plotted as line (b) in Fig. 5c the same as above. Compared the two plots calculated from (a) and (b), the slope of Fe_3O_4@PtTFPP@silane NPs is lower than that of Fe_3O_4@PtTFPP/C6@silane NPs. The slope of line (a) is 0.9059, which is larger than that of line (b), whose slope is 0.7658. As a result, adding C6 is much more beneficial to the oxygen sensitivity, because, in the composite, it serves as not only the reference probe, but also the sensitizer. Furthermore, Fe_3O_4@PtTFPP/C6@silane also shows remarkable reversibility and obtains a complete recovery in each time, as depicted in Fig. 5d.

The physiological process of oxygen consuming was also imitated. With constant concentration of glucose (8 mM), different concentration of glucose oxidase was added to the above solution to obtain an imitated hypoxia environment with various oxygen concentration. Fe_3O_4@PtTFPP/C6@silane NPs were added into the glucose solution in advance. The emission spectra of C6 and PtTFPP were tested before and after adding glucose oxidase, which could tune the oxygen consuming by catalyzing glucose degradation.

Firstly, glucose (8 mM, 100 μL) was added into a cuvette, containing Fe_3O_4@PtTFPP/C6@silane colloids. After adding glucose oxidase (1.4 mg mL^{-1}, 25 μL) into the former solution, the emission spectrum was measured immediately with one minute interval. As the line 1 shows, the intensity increases suddenly as adding glucose oxidase and keeps stable. At this point, glucose oxidase reacted with glucose instantly, and oxygen consuming happened and then the red emission intensity of oxygen-sensitive PtTFPP improved. Since the oxygen from air re-dissolved into the solution, the reaction arrived at a balance as the plateau describes.

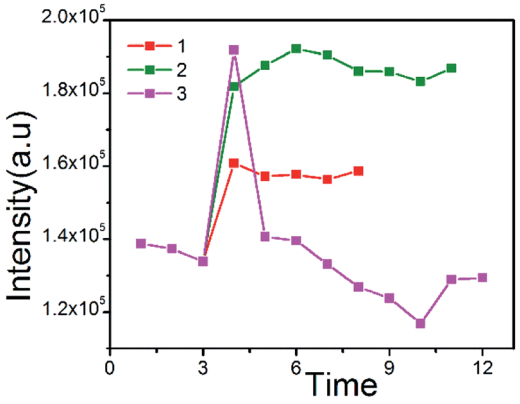

Fig. 6 The simplified physiological process of oxygen consuming was imitated through glucose (8 mM, 100 μL) and different amount of glucose oxidase, and DO sensing property was monitored with Fe_3O_4@PtTFPP/C6@silane NPs.

Similarly, when adding increasing amount of glucose oxidase (1.4 mg mL^{-1}, 50 μL), the line 2 was obtained, which showed the similar trend as the line 1, because the more glucose oxidase were introduced, the less oxygen remained in the solution. When overdose glucose oxidase was added into the solution, as the line 3 showed, glucose could be consumed more quickly, which caused remarkable DO consumption. Therefore, the peak of line 3 was much higher than 1 and 2. However, in this situation, the line 3 also had an obvious decline after adding overdose glucose oxidase, since the glucose was totally decomposed. Therefore, the re-desolved oxygen from air cause the rapid decline of the red emission of PtTFPP. These experiments were repeated for many times and fully proved the oxygen sensitivity of the Fe_3O_4@PtTFPP/C6@silane NPs by imitating the simplified physiological process of oxygen consuming (Fig. 6).

Cytotoxic effect of the core–shell sensing NPs

Before the intracellular oxygen sensing experiments, the potential cytotoxic effects are evaluated by using an MTT assay. The MTT assay is a colorimetric assay that measures the reduction of yellow 3-(4,5-dimethythiazol-2-yl)-2,5-diphenyltetrazolium bromide (MTT) by mitochondrial succinate dehydrogenase. MTT enters the cells and passes into the mitochondria where it is reduced to an insoluble colored (dark purple) formazan product. The cells are then solubilized with dimethyl sulfoxide and the released solubilised formazan reagent is measured spectrophotometrically. Therefore, it can be used to determine cytotoxicity of potential medicinal agents and toxic materials, since those agents would stimulate or inhibit cell viability and growth.

Fe_3O_4@PtTFPP/C6@silane colloids with concentration range from 8 to 40 μg mL^{-1} were incubated with MCF-7 cells for 12 h, and then the mitochondria and metabolic activities of the cells were examined after exposure to the complex of MTT. As shown in Fig. 7, introducing NPs with concentration of 40 μg mL^{-1} keeps the cell viability over 90%, showing good biocompatibility and low cytotoxicity to the cells.

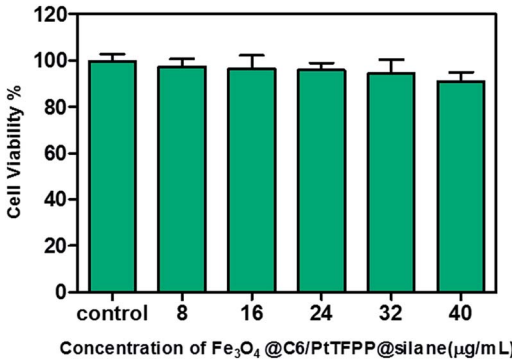

Fig. 7 MCF-7 cells viability determined by MTT assay. No significant difference between control and test groups is observed.

Intracellular oxygen sensitivity of the Fe_3O_4@PtTFPP/C6@silane NPs

Laser confocal scanning microscopy (LCSM) was employed here to investigate the ratiometric sensing NPs inside MCF-7 cells, as shown in Fig. S3.† As above mentioned, the fluorescence of the reference C6 (Fig. S3a†) and the probe PtTFPP (Fig. S3b†) were recorded by the green (475–550 nm) and red (620–680 nm) channels, respectively, under the same excitation of 458 nm laser, which is the standard configuration laser of LCSM. The dual fluorescence property suggests that intracellular oxygen sensing with the ratiometric nanosensors is possible.

To investigate the *in vitro* hypoxic response of Fe_3O_4@-PtTFPP/C6@silane NPs, the MCF-7 cells were incubated with NPs (40 μg mL^{-1}) for 24 h. Before oxygen sensing, glucose (8 mM, 100 μL) was pumped into the sealed confocal dish. The initial DO concentration was measured by the green and red emission signal. Then glucose oxidase (1.4 mg mL^{-1}, 50 μL) was added into the dish rapidly. The signals from both channels were monitored and the ratiometric gray intensity of the same point on the images were calculated. The images were captured every 10 seconds in 12 minutes after the introduction of oxidase. The gray intensity of signal was obtained from a selected area as the circle present.

Firstly, the correlation between red emission of PtTFPP and DO in cells was investigated. As the plot in Fig. 8a shows, red signal increases after the adding of glucose oxidase, due to the consumption of the DO inside the cells. The corresponding images of first and highest signal point (at 7 minute) from the red channel also indicate the remarkable improvement in signal intensity and resolution. At the highest point, consumption and re-dissolve of the oxygen come to the balance, and after that the signal decreases.

After the involvement of the stable green signal from C6 channel, the ratiometric fluorescence sensing can be achieved as the plot shows in Fig. 8b. Though the fluctuate of the gray intensity of the images is hard to avoid in the CLSM system, in this case, the ratiometric intensity between green and red channels shows more linear property relative to that from the single PtTFPP sensing method. Besides, ratiometric fluorescence sensing method also can bring an obvious improvement in sensitivity. In detail, at the beginning, the green fluorescence

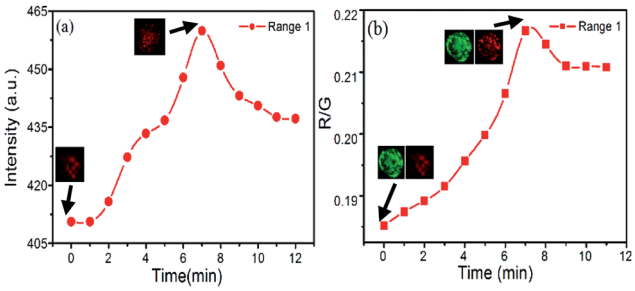

Fig. 8 (a) The red fluorescence emission intensity of Fe_3O_4@PtTFPP/C6@silane was plotted accompanied with experimental time, after adding glucose oxidase (1.4 mg mL^{-1}, 50 μL) into the dish. The insets were the corresponding areas. (b) The ratio of red fluorescence and green fluorescence (*R*/*G*) was plotted accompanied with experimental time after adding glucose oxidase (1.4 mg mL^{-1}, 50 μL) into the dish. The insets were the corresponding areas.

intensity from C6 is 2096.869 and the red fluorescence intensity from PtTFPP is 388.332. After 7 minutes, the maximum fluorescence intensity of both channels was achieved, which are 2275.784 and 480.1815 for red and green channels, respectively. By normalization of the green signal, the red signal behave a 14% increase. Also, the images corresponding to the first and highest points also support the signal variation. Therefore, though both the methods can be employed for the DO sensing, ratiometric fluorescence sensing shows better stability and sensitivity.

Magnetic targeting of Fe_3O_4@PtTFPP/C6@silane NPs

The cellar oxygen sensing is important in the tumor site or circulating tumor cells in blood, which are featured with hypoxia. Therefore, if magnetic navigation function can be integrated to the NPs, this multifunctional composites can be found more practical applications in clinic. In this work, the cell movement by Fe_3O_4@PtTFPP/C6@silane NPs was tested. As was shown in Fig. 9, a magnet was set near a cell culture dish with

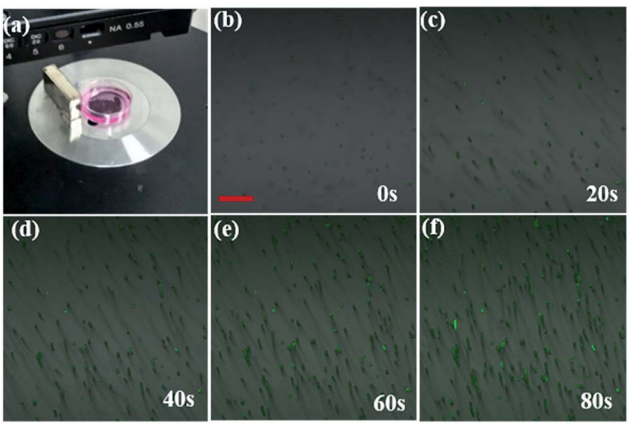

Fig. 9 MCF-7 cells intubated with Fe_3O_4@PtTFPP/C6@silane and then attracted to the lip of a Petri dish when the magnet was setting (a). (b) To (f) show the path and direction of the cells incubated with Fe_3O_4@PtTFPP/C6@silane NPs at different time by overlaying pictures. The scale bar is 200 μm.

MCF-7 cells incubated with Fe_3O_4@PtTFPP/C6@silane. After that, MCF-7 cells started to move along the magnetic field direction and the process was observed by CLSM. It can be seen that the movement traces could be described by pictures overlaid at 0, 20, 40, 60 and 80 s, indicating the efficient magnetic separation property. In addition, all the movements was monitored with green channel by the signal from C6. Therefore, the moving green cells suggest the *in vivo* applications with the imaging and magnetic functions, as well as the DO sensing property. The cell movement experiments under the CLSM was also carried using bright-field channel, and the moving process was monitored as a Video (ESI†). It is worthy to be mentioned here that the magnetic resonance imaging function can also be developed base on these Fe_3O_4@PtTFPP/C6@silane composite NPs.

Conclusions

We have developed the composite Fe_3O_4@PtTFPP/C6@silane NPs, which are suitable candidates with multifunctions of ratiometric fluorescence oxygen sensing, imaging and magnetic separation. The silane modification makes the composites stable and biocompatible. The efficient energy transfer from C6 to PtTFPP was proved, which greatly improve the DO sensing sensitivity and stability in imitation environment and *in vitro* experiments. Since C6 is not sensitive to oxygen, ratio metric emissions of C6 and PtTFPP can be employed here for precisely monitoring of oxygen concentration. The integration of magnetic property to the NPs, the composite with multifunction possess great potential in DO sensing related medical applications.

Acknowledgements

This work was supported by the National Key Research and Development Program (2016YFC0207101), Major State Basic Research Development Program of China (973 Program) (No. 2014CB643506), the program of Chang Jiang Scholars and Innovative Research Team in University (No. IRT13018) and the National Natural Science Foundation of China (Grant no. 11374127, 11304118, 81301289, 21403084 and 11674127) and National University Student Innovation Program (2016A51168).

Notes and references

1 T. Acker and H. Acker, *J. Exp. Biol.*, 2004, **207**, 3171.
2 J. Lopez-Barneo, R. Pardal and P. Ortega-Saenz, *Annu. Rev. Physiol.*, 2001, **63**, 259.
3 E. Ikeda, *Pathol. Int.*, 2005, **55**, 603.
4 R. Y. Zhang, R. R. Xing, T. F. Jiao, K. Ma, C. J. Chen, G. H. Ma and X. H. Yan, *ACS Appl. Mater. Interfaces*, 2016, **8**, 13262.
5 X. N. Zhao, K. Ma, T. F. Jiao, R. R. Xing, X. L. Ma, J. Hu, H. Huang, L. X. Zhang and X. H. Yan, *Sci. Rep.*, 2017, **7**, 44076.
6 Y. M. Liu, K. Ma, T. F. Jiao, R. R. Xing, G. Z. Shen and X. H. Yan, *Sci. Rep.*, 2017, **7**, 42978.
7 R. R. Xing, T. F. Jiao, Y. M. Liu, K. Ma, Q. L. Zou, G. H. Ma and X. H. Yan, *Polymers*, 2016, **8**, 181.
8 R. T. Xing, K. Liu, T. F. Jiao, N. Zhang, K. Ma, R. Y. Zhang, Q. L. Zou, G. H. Ma and X. H. Yan, *Adv. Mater.*, 2016, **28**, 3669–3676.
9 L. Galluzzi, E. Morselli, O. Kepp, I. Vitale, A. Rigoni, E. Vacchelli, M. Michaud, H. Zischka, M. Castedo and G. Kroemer, *Mol. Aspects Med.*, 2010, **31**, 1.
10 G. Kroemer and J. Pouyssegur, *Cancer Cell*, 2008, **13**, 472.
11 F. Giacco and M. Brownlee, *Circ. Res.*, 2010, **107**, 1058.
12 J. H. W. Distler, R. H. Wenger, M. Gassmann, M. Kurowska, A. Hirth, S. Gay and O. Distler, *Arthritis Rheum.*, 2004, **50**, 10.
13 J. N. Demas and B. A. Degraff, *Anal. Chem.*, 1991, **63**, 829A.
14 C. Preininger, I. Klimant and O. S. Wolfbeis, *Anal. Chem.*, 1994, **66**, 1841.
15 Z. Rosenzweig and R. Kopelman, *Anal. Chem.*, 1995, **67**, 2650.
16 C. McDonagh, B. D. MacCraith and A. K. McEvoy, *Anal. Chem.*, 1998, **70**, 45.
17 C. McDonagh, C. S. Burke and B. D. MacCraith, *Chem. Rev.*, 2008, **108**, 400.
18 F. Peng, Y. Y. Su, Y. L. Zhong, C. H. Fan, S. T. Lee and Y. He, *Acc. Chem. Res.*, 2014, **47**, 612.
19 X. D. Wang and O. S. Wolfbeis, *Chem. Soc. Rev.*, 2014, **43**, 3666.
20 Y. E. K. Lee, E. E. Ulbrich, G. Kim, H. Hah, C. Strollo, W. Fan, R. Gurjar, S. Koo and R. Kopelman, *Anal. Chem.*, 2010, **82**, 8446.
21 Y. Q. Gong, B. Yu, W. Yang and X. L. Zhang, *Biosens. Bioelectron.*, 2016, **79**, 822.
22 A. A. Khan, G. D. Vigil, Y. D. Zhang, S. K. Fullerton-Shirey and S. S. Howard, *Opt. Mater.*, 2017, **7**, 1066.
23 T. Yoshihara, Y. Hirakawa, M. Hosaka, M. Nangaku and S. Tobita, *J. Photochem. Photobiol., C*, 2017, **30**, 71.
24 E. R. Carraway, J. N. Demas, B. A. Degraff and J. R. Bacon, *Anal. Chem.*, 1991, **63**, 337.
25 A. Mills and A. Lepre, *Anal. Chem.*, 1997, **69**, 4653.
26 M. S. Tremblay, M. Halim and D. Sames, *J. Am. Chem. Soc.*, 2007, **129**, 7570.
27 X. D. Wang, X. Chen, Z. X. Xie and X. R. Wang, *Angew. Chem., Int. Ed.*, 2008, **47**, 7450.
28 X. D. Wang, T. Y. Zhou, X. H. Song, Y. Jiang, C. J. Yang and X. Chen, *J. Mater. Chem.*, 2011, **21**, 17651.
29 X. D. Wang, H. H. Gorris, J. A. Stolwijk, R. J. Meier, D. B. M. Groegel, J. Wegener and O. S. Wolfbeis, *Chem. Sci.*, 2011, **2**, 901.
30 X. H. Wang, H. S. Peng, H. Ding, F. T. You, S. H. Huang, F. Teng, B. Dong and H. W. Song, *J. Mater. Chem.*, 2012, **22**, 16066.
31 S. S. Lu, X. Wei, J. L. Zhang, Y. Y. Chen, L. Lei, Q. H. Yao, Y. Q. Jiang, Y. R. Wang and X. Chen, *Biosens. Bioelectron.*, 2016, **86**, 176.
32 K. A. Van Houten, D. C. Heath, C. A. Barringer, A. L. Rheingold and R. S. Pilato, *Inorg. Chem.*, 1998, **37**, 4647.
33 C. F. Wu, B. Bull, K. Christensen and J. McNeill, *Angew. Chem., Int. Ed.*, 2009, **48**, 2741.
34 X. H. Wang, H. S. Peng, L. Yang, F. T. You, F. Teng, L. L. Hou and O. S. Wolfbeis, *Angew. Chem., Int. Ed.*, 2014, **53**, 1.
35 J. L. Du, H. Y. Wang, L. Wang, S. J. Zhu, Y. B. Song, B. Yang and H. B. Sun, *J. Mater. Chem. C*, 2016, **4**, 2235.

